ACS Photonics

Article

pubs.acs.org/journal/apchd5

The Role of Plasmon-Generated Near Fields for Enhanced Circular Dichroism Spectroscopy

Maxim L. Nesterov,[‡] Xinghui Yin,[‡] Martin Schäferling, Harald Giessen, and Thomas Weiss*

4th Physics Institute and Research Center SCoPE, University of Stuttgart, 70550, Stuttgart, Germany

Supporting Information

ABSTRACT: Plasmon-enhanced circular dichroism has established itself as a promising candidate to push the limits of molecular handedness detection to the extremes, namely, toward a monolayer or even to a single molecule. A multitude of intricate mechanisms, both chemical and physical, have to contribute individually or in unison to an enhancement that is large enough that it may bridge the several orders of magnitude of lacking signal strength when detecting small analyte quantities in a circular dichroism scheme. Here, we assess in isolation the contribution arising from electromagnetic interactions between a homogeneous chiral medium and plasmonic structures. Using a suitably modified full-field electromagnetic simulation environment, we are able to investigate the viability of various canonical achiral and chiral plasmonic configurations for substrate-enhanced chiroptical spectroscopy. A clear hierarchy in enhancement factors is revealed that places achiral plasmonic gap antennas at the top, thus outperforming its chiral equivalent, the Born−Kuhn-type plasmonic dimer. Moreover, the importance of coplanarity of the incident rotating circular polarization field vector with the resonantly enhanced field vector in the plasmonic hot-spot is demonstrated. Taking everything into account, we obtain an enhancement of 3 orders of magnitude from purely electromagnetic interactions, thereby charting this part of the CD enhancement landscape.

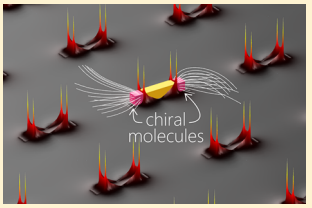

KEYWORDS: *chiroptical spectroscopy, bi-isotropic, plasmonics, enhanced, sensing*

Surface plasmon-based near-field enhancement delivered through specifically designed substrates has proven to be highly successful for ultrasensitive optical biosensor applications such as surface-enhanced Raman spectroscopy (SERS)[1] and surface-enhanced infrared absorption (SEIRA),[2] where it can boost responses down to the monolayer and even to the single-molecule regimes.[3] The underlying detection schemes record the changes in intensity of the probing light, regardless of its polarization. However, taking the aspect of polarization into account provides valuable additional information which is precisely the domain of chiroptical spectroscopy techniques that are sensitive to the chirality[4] (handedness) of a molecule. Among these, circular dichroism (CD), i.e., differential absorption of left- and right-handed circularly polarized light, is of particular relevance for the study of biomolecules. Apart from being able to unambiguously distinguish the enantiomers of a chiral molecule, it can precisely determine the macroscopic conformation of large complex molecules.[5] As these molecules are prevalent in pharmaceutical applications,[6] it is of great importance to be able to operate chiral analyses at physiological—hence very low—concentrations. Recently, experimental[7,8] and theoretical[9,10] work has been carried out on plasmon-enhanced circular dichroism spectroscopy, reporting dissymmetry enhancement factors of up to 10^5 and attributed to plasmon-generated superchiral near fields[11−18] or induced optical activity due to near fields, both at isolated plasmonic nanostructures and at hot-spots between closely spaced structures.[19−26] This substrate-based approach is akin to SERS and SEIRA but fundamentally differs from routes to enhanced circular dichroism that rely on self-assembled chiral plasmonic macrostructures. The latter approach judiciously incorporates the analyte as part of the scaffolding material for the nanoparticles, thus influencing the geometrical configuration of the chiral plasmonic structure and thereby its associated CD spectrum.[27−29]

While previous theoretical work focused on either investigating a fixed number of chiral molecules modeled as point dipoles[19,20,30] or analyzing optical chirality in the vicinity of plasmonic nanostructures by using Mie calculations[9] or full-field simulations, so far, comprehensive three-dimensional numerical studies encompassing both the plasmonic structure and chiral molecular material have not been carried out. It has been shown, however, that chiral media can be treated with chiral Mie theory[31] and full-field simulations.[32,33]

Here, we present, for the first time, a rigorous finite element method based study on the effects of various canonical plasmonic building blocks on the enhancement of molecular CD signals. Full-field simulations that take both the complex plasmonic structure and the chiral medium into account reveal the importance of highly concentrated near fields. Most importantly, we demonstrate that the relative orientation between incident light and plasmonic modes plays a crucial role. This leads to rather counterintuitive consequences for the performance of different plasmonic antenna shapes where achiral structures clearly outperform their chiral equivalents.

The investigated structures consist of homogeneous and isotropic chiral medium patches placed in the vicinity of

Received: November 10, 2015
Published: March 14, 2016

DOI: 10.1021/acsphotonics.5b00637
ACS Photonics 2016, 3, 578−583

plasmonic nanoantennas, with the molecular resonance of the chiral medium patches in the UV range and the plasmonic resonance in the near-IR. Our numerical approach contains all electromagnetic effects that can contribute to an enhancement of the CD signal of the chiral medium patches, while other effects, e.g., of chemical nature such as charge transfer through bonds formed by chemisorbed analytes to the plasmonic nanostructure, are not considered. An extension to oriented chiral molecules by using anisotropic material tensors as well as the investigation of matched molecular and plasmonic resonances is in principle possible, but we focus here on the more common case, in which the molecular and the plasmonic resonance are spectrally separated and the molecules are randomly oriented.

The general setup for plasmon-enhanced circular dichroism spectroscopy (PECD) employs a standard CD detection scheme in conjunction with arbitrarily shaped plasmonic nanoantennas as a substrate for the chiral material (Figure 1).

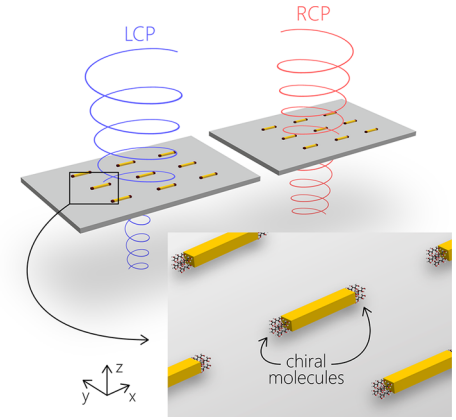

Figure 1. Schematic of plasmon-enhanced circular dichroism (PECD) detection scheme. The inset shows the chiral material patches that are placed at the hot-spots of the plasmonic antennas.

Ideally, the material under investigation should be placed in the hot-spot regions of the nanoparticles in order to assess the upper limit for the obtainable plasmon enhancement.

While it is straightforward to model the linear optical response of plasmonic materials such as gold, the electromagnetic behavior of chiral media, a subset of bi-isotropic media, requires some adaptation of existing commercial Maxwell solvers. For our studies of PECD, we chose to modify a standard COMSOL RF simulation environment by implementing chiral constitutive equations:

$$\mathbf{D} = \varepsilon_0 \varepsilon \mathbf{E} - \frac{i\kappa}{c}\mathbf{H}$$
$$\mathbf{B} = \mu_0 \mu \mathbf{H} + \frac{i\kappa}{c}\mathbf{E} \quad (1)$$

where ε and μ denote permittivity and permeability, respectively, and κ is used for the Pasteur parameter that controls the coupling between electric and magnetic responses of the medium and, therefore, the strength of its chirality. The parameters are modeled as[32]

$$\varepsilon = \varepsilon_b - \gamma\left(\frac{1}{\hbar\omega - \hbar\omega_0 + i\Gamma} - \frac{1}{\hbar\omega + \hbar\omega_0 + i\Gamma}\right)$$
$$\kappa = \beta\left(\frac{1}{\hbar\omega - \hbar\omega_0 + i\Gamma} - \frac{1}{\hbar\omega + \hbar\omega_0 + i\Gamma}\right)$$
$$\mu = 1 \quad (2)$$

where ε_b denotes the background refractive index and the coefficients γ and β are the amplitude of absorptive and chiral properties; $\omega_0 = 2\pi c/\lambda_0$, where λ_0 corresponds to the wavelength of a molecular absorption resonance with broadening determined through damping Γ. Furthermore, the chiral medium is assumed to be nonmagnetic with $\mu = 1$. The values for all other parameters were chosen to represent typical values found in naturally occurring neat, i.e., 100% concentration, chiral materials[5] (cf. Supporting Information S1). The various optical responses (Figure 2) of the system employing

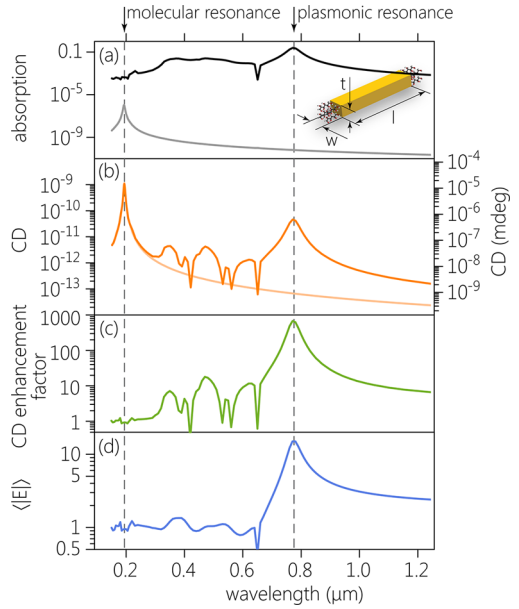

Figure 2. Optical responses of chiral medium patches located at the hot-spots of a plasmonic rod antenna array. Paler lines indicate the chiral response of the patches without antennas. (a) Absorption for linearly polarized normal incidence. (b) Circular dichroism signal (absolute values). The scale on the right marks CD values as ellipticity in millidegrees. (c) Enhancement factor of the CD signal. (d) Averaged electric field enhancement within the volume occupied by the chiral patches.

periodically arranged gold rod structures shown in Figure 1 illustrate the key features of PECD spectroscopy. The rods have a length l = 150 nm, a width w = 40 nm, and a thickness t = 40 nm, and they are arranged in an array of period p = 650 nm in both directions of the plane. Typically, molecular CD resonances of interest are located around 200 nm, while the utilized plasmonic structures exhibit their fundamental resonance at longer wavelengths, here at 780 nm, such that no spectral overlap of the absorption peaks occurs (Figure 2a). The black line in Figure 2a shows the absorption spectrum of the compound system, whereas the gray curve corresponds to the absorption from the chiral medium patches by themselves. The spectral features that are visible in the region between the molecular and fundamental plasmonic resonance stem from

DOI: 10.1021/acsphotonics.5b00637
ACS Photonics 2016, 3, 578−583

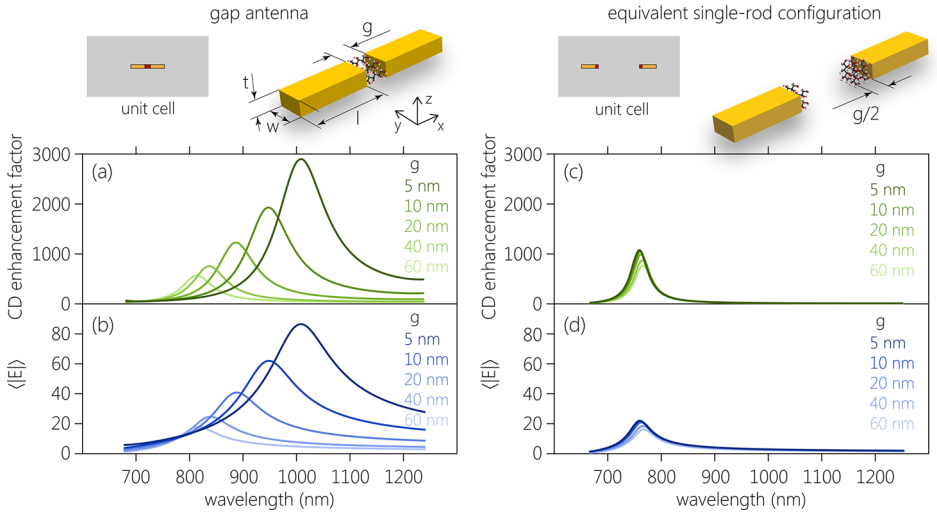

Figure 3. Gap antenna and rod antenna enhancement factors. (a) CD enhancement factor for gap antennas of different gap sizes. (b) Averaged field enhancement within the volume occupied by the chiral medium in the case of gap antennas. (c) CD enhancement factor of the equivalent single rod antenna configuration for varying chiral medium volumes with side length g. (d) Averaged field enhancement within the volume occupied by the chiral medium in the case of rod antennas.

Rayleigh modes and higher order plasmon modes, which we do not further investigate here.

The CD peak for the chiral patches is naturally located at the spectral location of their molecular absorption resonance (Figure 2b). Note the weakness of the CD signal of about 10^{-4} mdeg at its maximum, despite assuming neat liquid model parameters. This results from the small analyte quantity involved, i.e., 40 nm sized chiral medium cubes instead of uniform millimeter thick analyte layers that are usually required for unenhanced CD spectroscopy, where the detection limit is typically about 1 mdeg.

The achiral plasmonic nanorods inherently do not exhibit a CD signal. However, due to the presence of the chiral material that interacts with the near fields of the rods, a difference in absorption for left- and right-handed circularly polarized (LCP and RCP) illumination is induced inside the metal nanoparticles. This difference manifests itself as a CD signal at the position of the plasmon resonance (orange plot Figure 2b). Generally, CD signals can take positive and negative values depending on the handedness of the examined sample; here, we present only the absolute values as we concentrate on determining enhancement effects that occur symmetrically for opposite enantiomers.

In order to quantify such enhancement phenomena, we define the CD enhancement factor f as the ratio between the absolute values of the CD signal of the chiral medium patches alone and with plasmonic antennas. Note that this definition only accounts for the enhancement of the CD signal for a fixed size and position of the chiral patches at a certain wavelength. In order to obtain larger total CD signals, it is of course possible to increase the size of the chiral patches. However, investigating chiral patches that extend the region of the plasmonic near fields does not reveal any enhancement effects due to the plasmonic resonances. Plotting the CD enhancement factor for the case of the plasmonic nanorod array with chiral patches provides a maximum enhancement factor of about 750 (Figure 2c). It is important to note that this enhancement factor is independent of the magnitude of the Pasteur parameter κ as long as it is small with respect to the dielectric permittivity, which is usually the case for realistic chiral analytes. Therefore, our results reveal fundamental insights independent of the actual properties of the chiral medium.

The enhancement effect is clearly tied in with the effect of field enhancement that can be observed at the ends of the metal nanorods. Figure 2d shows the electric field enhancement $\langle|E|\rangle$, which has been calculated by averaging the absolute electric field value $|\mathbf{E}|$ over the volume V occupied by the chiral medium cubes and normalizing to the amplitude E_0 of the incident electric field:

$$\langle|E|\rangle = \frac{1}{V}\int_V \frac{|\mathbf{E}|}{E_0} dV \tag{3}$$

In the Supporting Information, we additionally analyze the origin of the enhanced CD signals by distinguishing between energy absorbed in the metallic nanoantenna and in the chiral medium patches. We find that the CD signal is dominated by the contribution of the nanoantenna, so that the most relevant mechanism is the so-called induced CD.[20] Note, however, while the CD enhancement obtained for the present case of plasmonic rod antenna arrays is an undeniably large effect, it still yields an overall CD signal below the detection limit of 1 mdeg for common CD spectrometers.

Therefore, we carried out numerical studies of variations of the basic rod antenna geometry to assess whether higher CD enhancement factors can be obtained.

As near-field concentration plays a crucial role, the next iteration of the rod antenna geometry is the gap antenna, i.e., two rod antennas aligned along their long axes such that they are interacting through the near fields at the junction formed between them. In the gap region, the field enhancement is larger than at the ends of a rod antenna alone.[34] We studied the geometries presented in Figure 3: the gap antenna has dimensions l = 150 nm, w = 40 nm, and t = 40 nm with gap sizes g varying from 5 to 60 nm. The gap region is fully occupied by the chiral medium; that is, its dimensions are 40 nm × 40 nm × g. The antennas are arranged periodically with period p_x = 1300 nm and p_y = 650 nm.

In order to directly compare the gap antenna CD enhancement factors to those obtained from a single rod

DOI: 10.1021/acsphotonics.5b00637
ACS Photonics 2016, 3, 578−583

antenna, we used an equivalent geometry that does not exhibit gap hot-spots by placing two rod antennas at a distance from one another that is sufficient to avoid near-field coupling. In particular, the end-to-end distance between the two rods was chosen to be 175 nm. The chiral medium volume was cut in half for this geometry compared to that employed for the gap antenna, with one-half patch each being placed at the ends of the rod antennas that face each other. As expected, the field enhancement for the gap antenna is higher than for the single rod antenna. For the smallest gap size of g = 5 nm, the gap antenna field enhancement is 4 times higher than for single rod antennas. In this case, the highest CD enhancement factor ratio is achieved between the two systems. The gap antenna exhibits a CD enhancement factor of 3000, and the equivalent single-rod configuration yields only one-third of that with a CD enhancement factor of about 1000.

The average field and CD enhancement factors show a slight increase for the single-rod geometry as the chiral medium patch size decreases, which happens due to the fact that the near fields are stronger closer to the antenna surface. Consequently, PECD enhancement benefits are more pronounced for small judiciously placed chiral analyte patches and decrease when using continuous analyte layers, because the chiral material outside the near-field regions of the plasmonic antennas does not contribute to an enhanced CD signal.

It should be mentioned that the gap antennas with gaps of 40 and 60 nm provide slightly lower CD enhancement than equivalent single rod configurations. We attribute this to the more efficient excitation of higher diffraction orders by the gap antenna as compared to single rods, which results in a nontrivial redistribution of radiation to the far field. However, a detailed discussion of the influence of higher diffraction orders and other grating effects on the CD enhancement is beyond the scope of this paper.

Furthermore, we tested if the chiral equivalent of the gap antenna dimer, i.e., a Born−Kuhn-type chiral dimer,[35] yields higher CD enhancement factors (Figure 4). We used the same dimensions as before for the rods that constitute the chiral dimer with l = 150 nm, w = 40 nm, t = 40 nm, and vertically varying gap sizes g. The chiral dimer itself already possesses a CD signal that would appear as background in the PECD measurement. Therefore, the CD enhancement factors presented in Figure 4a were obtained from baseline-corrected CD signals (Supporting Information S2). Due to mode hybridization, a bonding and antibonding mode can be excited depending on the handedness of the incident illumination. Here, we present the results for a left-handed dimer for which the field enhancement in the gap region is slightly larger for RCP light (Figure 4b) and comparable to that obtained for the achiral gap antenna. However, the CD enhancement factor is 1 order of magnitude lower than in the previously considered case of the gap antenna (Figure 4a).

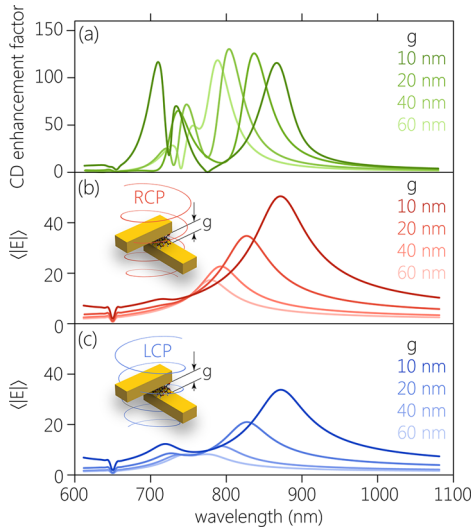

Figure 4. Chiral plasmonic dimers with chiral medium patches placed in their hot-spot region. (a) CD enhancement factor for different gap sizes. (b and c) Averaged electric field enhancement within the hot-spots of the plasmonic dimers for RCP and LCP incident light, respectively.

The significant drop in CD enhancement for the chiral dimer can be explained by considering the intermediate geometrical configurations schematically shown in Figure 5 on the left. The chiral cubic patches have the same dimensions as before with g_x = g_z = 40 nm. The planar gap antenna delivers the highest CD enhancement, which drops to about half its value for the second geometry from the top, where one of the rod antennas has been vertically lifted out of the plane. This value further decreases by an order of magnitude when the ends of the nanorods overlap (Figure 5a). The average field enhancement, however, drops only roughly by a factor of 2. *This indicates that the relative orientation of the incident electric field vector and the electric field vector in the hot-spot region is of great importance for plasmon-enhanced CD signals.* While the standard gap antennas possess hot-spot electric field vectors that are parallel to the incident electric field vector, this is not true for the other two cases. In particular, the hot-spot and incident field vectors are mostly orthogonal to each other for the gap antenna where the ends are overlapping each other (Figure 5 right side), which likely causes the dramatic reduction of the CD enhancement effect.

In summary, we studied the contribution of macroscopic electromagnetic effects to plasmon-enhanced CD spectroscopy. To this end, we implemented chiral constitutive equations in the COMSOL RF simulation environment. The highest enhancement factor is achieved for the standard planar gap antenna, which outperforms both the single rod antenna and its chiral equivalent, the Born-Kuhn-type dimer. Careful analysis of intermediate geometries revealed the pivotal role that the mutual orientation of incident and hot-spot electric field vectors plays. In our findings, CD enhancement is highest for geometries where these field vectors are parallel to one another and when, simultaneously, the average field enhancement value is high. The large CD enhancement of roughly 3 orders of magnitude constitutes the electromagnetic contribution to plasmon-enhanced CD spectroscopy. The limiting aspect here lies in the small volumes occupied by enhanced near fields at the hot-spots of plasmonic antennas. Only in these regions does electromagnetic CD enhancement occur.

It should be noted that in the cases without any additional alignment effects or chemical enhancement[36] that may occur for chemisorbed analytes and are strongly analyte dependent, it might be more practical to measure the molecular resonance directly in the ultraviolet spectral region when employing a substrate-based enhancement scheme, as the molecular CD resonance remains stronger than the induced CD signal at 780 nm in absolute terms. The ratio between the maximum values of induced CD (at the plasmonic resonance) and molecular CD (without plasmonic nanoantenna at the molecular resonance) reaches about 0.04 for the rod antenna and 0.17−0.52 for the

DOI: 10.1021/acsphotonics.5b00637
ACS Photonics 2016, 3, 578−583

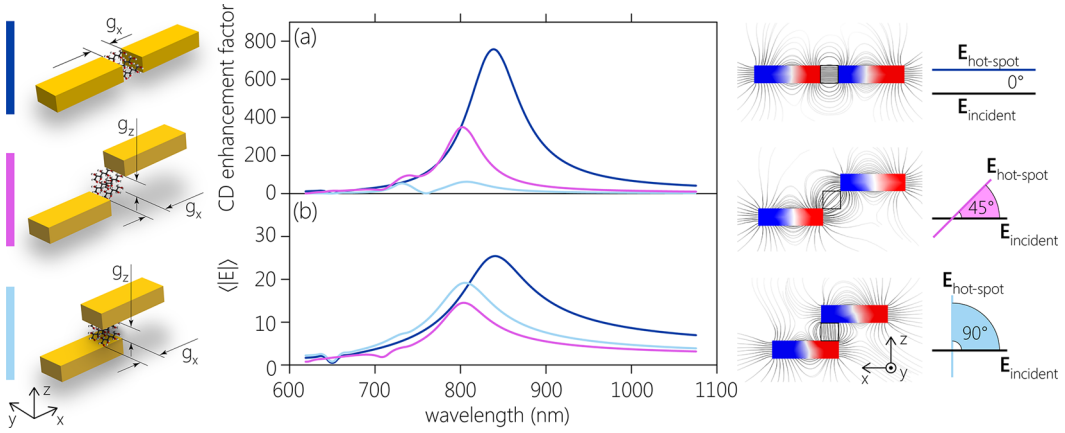

Figure 5. Enhancement factors for different dimer configurations (geometries are schematically shown on the left). (a) CD enhancement factor. (b) Electric field enhancement factor within the hot-spot regions. On the right, electric field lines and charge distributions are depicted at the resonance wavelength.

gap antenna with gap sizes of 60−5 nm, respectively. Only in those cases where one is restricted to typical plasmon resonance wavelengths for detection is a pure electromagnetic plasmon-enhanced CD scheme advantageous for measuring the CD signal from small patches of chiral media at the hot-spots of the electric fields.

The present thorough analysis is an important step toward dissecting the different contributing effects involved in plasmonic substrate-based CD enhancement schemes. As with SERS, large overall enhancement in plasmon-enhanced CD is expected to be composed of both physical and chemical parts. Note that the contribution of the chemical part may be relevant in experiments, but it is beyond the scope of this work to discuss the potentially involved mechanisms as well as to estimate the magnitude of the resulting CD enhancement due to the chemical effects.

While the determined electromagnetic enhancement of 3 orders of magnitude does not strictly represent an upper bound, it is reasonable to assume that for homogeneous and isotropic chiral medium patches the present numerical results give a good estimate of the maximally experimentally achievable CD enhancement based on electromagnetic effects. This is due to our finding that high field enhancement, which is challenging to achieve in real devices, is the overall limiting factor.

Despite assuming the chiral medium patches to be homogeneous and isotropic here, future work will also include molecular orientation effects that can be easily implemented in our numerical method by using tensorial parameters. Such additional detail might very well reveal even higher electromagnetic enhancement factors.

METHODS

The results presented here are based on the numerical solution of Maxwell's equations incorporating the constitutive eqs 1 for the chiral medium. We used the commercial finite element method software COMSOL Multiphysics.

Materials. The bulk dielectric function for gold is fitted using a phenomenological Brendel−Bormann model.[37] The chiral medium is determined by complex dispersive isotropic macroscopic parameters: dielectric permittivity ε, magnetic permeability $\mu = 1$, and Pasteur parameter κ (Supporting Information (S1)).

Mesh. To adequately resolve the electromagnetic effects, we chose at least five tetrahedral elements with second-order shape functions per local wavelength. At least two second-order elements were used to resolve the field variations occurring within the skin depth at the surface of the metal. A denser mesh was generated in the near-field regions at the hot-spots to register the weak chiral signals from the chiral medium. Each simulation was checked for convergence.

CD Enhancement Factors. Circular dichroism is calculated as a difference in absorption of left-handed and right-handed circularly polarized incident light: $CD = A_{RCP} - A_{LCP}$. To obtain the CD enhancement factor, we normalize the CD signal from the combined plasmon-chiral medium system by the CD signal of the chiral medium itself at the same wavelength: $f = |CD_{total}|/|CD_{chiral\ medium}|$.

ASSOCIATED CONTENT

Supporting Information

The Supporting Information is available free of charge on the ACS Publications website at DOI: 10.1021/acsphotonics.5b00637.

Performance tests of modified simulation environment; chiral material models, loss decomposition, and parameter fits (PDF)

AUTHOR INFORMATION

Corresponding Author

*E-mail: t.weiss@pi4.uni-stuttgart.de.

Author Contributions

‡M. L. Nesterov and X. Yin contributed equally.

Notes

The authors declare no competing financial interest.

ACKNOWLEDGMENTS

The authors would like to thank Thorsten Schuhmacher for initial support with the implementation of chiral media. The authors gratefully acknowledge financial support by the ERC Advanced Grant (COMPLEXPLAS), BMBF (13N9048 and 13N10146), the Baden-Württemberg Stiftung (Internationale Spitzenforschung II), the MWK Baden-Württemberg (Zukunft-soffensive IV), and DFG (SPP1391, FOR730). M.N. acknowledges support by the Alexander-von-Humboldt foundation. X.Y. additionally acknowledges financial support by the Carl-Zeiss-Stiftung.

DOI: 10.1021/acsphotonics.5b00637
ACS Photonics 2016, 3, 578−583

REFERENCES

(1) Stiles, P. L.; Dieringer, J. A.; Shah, N. C.; Van Duyne, R. R. Surface-Enhanced Raman Spectroscopy. *Annu. Rev. Anal. Chem.* **2008**, *1*, 601−626.

(2) Neubrech, F.; Pucci, A.; Cornelius, T. W.; Karim, S.; Garcia-Etxarri, A.; Aizpurua, J. Resonant Plasmonic and Vibrational Coupling in a Tailored Nanoantenna for Infrared Detection. *Phys. Rev. Lett.* **2008**, *101*, 157403.

(3) Li, M.; Cushing, S. K.; Wu, N. Plasmon-Enhanced Optical Sensors: a Review. *Analyst* **2014**, *140*, 386−406.

(4) Kelvin, B. W. T. *Baltimore Lectures on Molecular Dynamics and the Wave Theory of Light*; CJ Clay and Sons, 1904.

(5) Fasman, G. D. *Circular Dichroism and the Conformational Analysis of Biomolecules*, 1st ed.; Fasman, G. D., Fasman, E. B., Eds.; Springer, 2010.

(6) Nguyen, L. A.; He, H.; Pham-Huy, C. Chiral Drugs: an Overview. *Int. J. Biomed. Sci.: IJBS* **2006**, *2*, 85−100.

(7) Hendry, E.; Carpy, T.; Johnston, J.; Popland, M.; Mikhaylovskiy, R. V.; Lapthorn, A. J.; Kelly, S. M.; Barron, L. D.; Gadegaard, N.; Kadodwala, M. Ultrasensitive Detection and Characterization of Biomolecules Using Superchiral Fields. *Nat. Nanotechnol.* **2010**, *5*, 783−787.

(8) Tullius, R.; Karimullah, A. S.; Rodier, M.; Fitzpatrick, B.; Gadegaard, N.; Barron, L. D.; Rotello, V. M.; Cooke, G.; Lapthorn, A.; Kadodwala, M. "Superchiral" Spectroscopy: Detection of Protein Higher Order Hierarchical Structure with Chiral Plasmonic Nanostructures. *J. Am. Chem. Soc.* **2015**, *137*, 8380−8383.

(9) Garcia-Etxarri, A.; Dionne, J. A. Surface-Enhanced Circular Dichroism Spectroscopy Mediated by Nonchiral Nanoantennas. *Phys. Rev. B: Condens. Matter Mater. Phys.* **2013**, *87*, 235409.

(10) Davis, T. J.; Gomez, D. E. Interaction of Localized Surface Plasmons with Chiral Molecules. *Phys. Rev. B: Condens. Matter Mater. Phys.* **2014**, *90*, 235424.

(11) Tang, Y.; Cohen, A. E. Optical Chirality and Its Interaction with Matter. *Phys. Rev. Lett.* **2010**, *104*, 163901.

(12) Tang, Y.; Cohen, A. E. Enhanced Enantioselectivity in Excitation of Chiral Molecules by Superchiral Light. *Science* **2011**, *332*, 333−336.

(13) Schäferling, M.; Yin, X.; Giessen, H. Formation of Chiral Fields in a Symmetric Environment. *Opt. Express* **2012**, *20*, 26326−26336.

(14) Schäferling, M.; Yin, X.; Engheta, N.; Giessen, H. Helical Plasmonic Nanostructures as Prototypical Chiral Near-Field Sources. *ACS Photonics* **2014**, *1*, 530−537.

(15) Schäferling, M.; Dregely, D.; Hentschel, M.; Giessen, H. Tailoring Enhanced Optical Chirality: Design Principles for Chiral Plasmonic Nanostructures. *Phys. Rev. X* **2012**, *2*, 031010.

(16) Hendry, E.; Mikhaylovskiy, R. V.; Barron, L. D.; Kadodwala, M.; Davis, T. J. Chiral Electromagnetic Fields Generated by Arrays of Nanoslits. *Nano Lett.* **2012**, *12*, 3640−3644.

(17) Meinzer, N.; Hendry, E.; Barnes, W. L. Probing the Chiral Nature of Electromagnetic Fields Surrounding Plasmonic Nanostructures. *Phys. Rev. B: Condens. Matter Mater. Phys.* **2013**, *88*, 041407.

(18) Davis, T. J.; Hendry, E. Superchiral Electromagnetic Fields Created by Surface Plasmons in Nonchiral Metallic Nanostructures. *Phys. Rev. B: Condens. Matter Mater. Phys.* **2013**, *87*, 085405.

(19) Govorov, A. O.; Fan, Z.; Hernandez, P.; Slocik, J. M.; Naik, R. R. Theory of Circular Dichroism of Nanomaterials Comprising Chiral Molecules and Nanocrystals: Plasmon Enhancement, Dipole Interactions, and Dielectric Effects. *Nano Lett.* **2010**, *10*, 1374−1382.

(20) Govorov, A. O. Plasmon-Induced Circular Dichroism of a Chiral Molecule in the Vicinity of Metal Nanocrystals. Application to Various Geometries. *J. Phys. Chem. C* **2011**, *115*, 7914−7923.

(21) Abdulrahman, N. A.; Fan, Z.; Tonooka, T.; Kelly, S. M.; Gadegaard, N.; Hendry, E.; Govorov, A. O.; Kadodwala, M. Induced Chirality Through Electromagnetic Coupling Between Chiral Molecular Layers and Plasmonic Nanostructures. *Nano Lett.* **2012**, *12*, 977−983.

(22) Maoz, B. M.; Chaikin, Y.; Tesler, A. B.; Bar Elli, O.; Fan, Z.; Govorov, A. O.; Markovich, G. Amplification of Chiroptical Activity of Chiral Biomolecules by Surface Plasmons. *Nano Lett.* **2013**, *13*, 1203−1209.

(23) Maoz, B. M.; van der Weegen, R.; Fan, Z.; Govorov, A. O.; Ellestad, G.; Berova, N.; Meijer, E. W.; Markovich, G. Plasmonic Chiroptical Response of Silver Nanoparticles Interacting with Chiral Supramolecular Assemblies. *J. Am. Chem. Soc.* **2012**, *134*, 17807−17813.

(24) Lu, F.; Tian, Y.; Liu, M.; Su, D.; Zhang, H.; Govorov, A. O.; Gang, O. Discrete Nanocubes as Plasmonic Reporters of Molecular Chirality. *Nano Lett.* **2013**, *13*, 3145−3151.

(25) Wang, R.-Y.; Wang, P.; Liu, Y.; Zhao, W.; Zhai, D.; Hong, X.; Ji, Y.; Wu, X.; Wang, F.; Zhang, D.; Zhang, W.; Liu, R.; Zhang, X. Experimental Observation of Giant Chiroptical Amplification of Small Chiral Molecules by Gold Nanosphere Clusters. *J. Phys. Chem. C* **2014**, *118*, 9690−9695.

(26) Govorov, A. O.; Gun'ko, Y. K.; Slocik, J. M.; Gerard, V. A.; Fan, Z.; Naik, R. R. Chiral Nanoparticle Assemblies: Circular Dichroism, Plasmonic Interactions, and Exciton Effects. *J. Mater. Chem.* **2011**, *21*, 16806−16818.

(27) Ma, W.; Kuang, H.; Xu, L.; Ding, L.; Xu, C.; Wang, L.; Kotov, N. A. Attomolar DNA Detection with Chiral Nanorod Assemblies. *Nat. Commun.* **2013**, *4*, 2689.

(28) Xu, Z.; Xu, L.; Liz Marzán, L. M.; Ma, W.; Kotov, N. A.; Wang, L.; Kuang, H.; Xu, C. Sensitive Detection of Silver Ions Based on Chiroplasmonic Assemblies of Nanoparticles. *Adv. Opt. Mater.* **2013**, *1*, 626−630.

(29) Zhao, Y.; Xu, L.; Ma, W.; Wang, L.; Kuang, H.; Xu, C.; Kotov, N. A. Shell-Engineered Chiroplasmonic Assemblies of Nanoparticles for Zeptomolar DNA Detection. *Nano Lett.* **2014**, *14*, 3908−3913.

(30) Wu, T.; Ren, J.; Wang, R.; Zhang, X. Competition of Chiroptical Effect Caused by Nanostructure and Chiral Molecules. *J. Phys. Chem. C* **2014**, *118*, 20529−20537.

(31) Govorov, A. O.; Fan, Z. Theory of Chiral Plasmonic Nanostructures Comprising Metal Nanocrystals and Chiral Molecular Media. *ChemPhysChem* **2012**, *13*, 2551−2560.

(32) Klimov, V. V.; Zabkov, I. V.; Pavlov, A. A.; Guzatov, D. V. Eigen Oscillations of a Chiral Sphere and Their Influence on Radiation of Chiral Molecules. *Opt. Express* **2014**, *22*, 18564−18578.

(33) Onishi, M.; Crabtree, K.; Chipman, R. A. Formulation of Rigorous Coupled-Wave Theory for Gratings in Bianisotropic Media. *J. Opt. Soc. Am. A* **2011**, *28*, 1747−1758.

(34) Dregely, D.; Neubrech, F.; Duan, H.; Vogelgesang, R.; Giessen, H. Vibrational Near-Field Mapping of Planar and Buried Three-Dimensional Plasmonic Nanostructures. *Nat. Commun.* **2013**, *4*, 2237.

(35) Yin, X.; Schäferling, M.; Metzger, B.; Giessen, H. Interpreting Chiral Nanophotonic Spectra: the Plasmonic Born−Kuhn Model. *Nano Lett.* **2013**, *13*, 6238−6243.

(36) Le Ru, E. C.; Etchegoin, P. G. Quantifying SERS enhancements. *MRS Bull.* **2013**, *38*, 631−640.

(37) Rakic, A.; Djurisic, A.; Elazar, J.; Majewski, M. Optical Properties of Metallic Films for Vertical-Cavity Optoelectronic Devices. *Appl. Opt.* **1998**, *37*, 5271−5283.

DOI: 10.1021/acsphotonics.5b00637
ACS Photonics 2016, 3, 578−583